Integrating ANSYS Mechanical Analysis with Optical Performance Analysis Using SigFit

Gregory J. Michels, Victor L. Genberg, Keith B. Doyle

Sigmadyne, Inc., Rochester, NY, USA

Summary

The development of products in many industries requires the application of multiple disciplines of engineering in order to obtain useful performance predictions. In the photonics industry performance degradations are caused by various mechanical disturbances such as deformations, motions, temperature changes, and induced stresses within optical components and the metering structures that support them. However, mechanical predictions from finite element tools are not in a readily useable form for use in optical performance analysis tools. This paper discusses the integration of mechanical finite element analysis and optical performance analysis that is required to recast ANSYS results output into a useable format for some common commercially available optical analysis tools. Also discussed is the generation of optical absorption thermal loading descriptions for finite element analysis. Specific mechanical disturbance issues include optical surface deformations, thermo-optic effects, and stress-induced birefringence effects. Optical surface deformations derived from nodal displacements predicted by ANSYS analysis tools are fit to several polynomial types including Zernike, aspheric, and XY. Deformations with higher spatial frequency content are interpolated to a user-defined uniform grid array using element shape functions to create interferogram files or grid sag surfaces. Three-dimensional shape function interpolation is used to develop integrated maps of optical path difference and birefringence due to thermo-optic effects (dn/dT) and induced stresses, respectively, which may be used for subsequent optical performance analysis. The resulting capability of making optical performance predictions that are tightly linked with mechanical performance predictions from ANSYS allows opto-mechanical engineers to achieve more aggressive performance requirements.

Keywords

multidisciplinary, optomechanics, optic, dndT, thermo-optic, stress, birefringence

1. Introduction

A flow chart of the process of optomechanical analysis of an optical system using ANSYS and SigFit is shown in Figure 1.1 [1,2]. Thermal and mechanical loads are applied to a finite element model constructed in ANSYS for the purpose of predicting displacements, temperatures, and stresses in the optical components. These finite element results are subsequently processed by SigFit to generate result files which are importable into commercially available optical analysis tools. These optical analysis tools can then be used to make optical performance predictions which are meaningful to optical engineers yet based on well predicted mechanical behavior of the optical system.
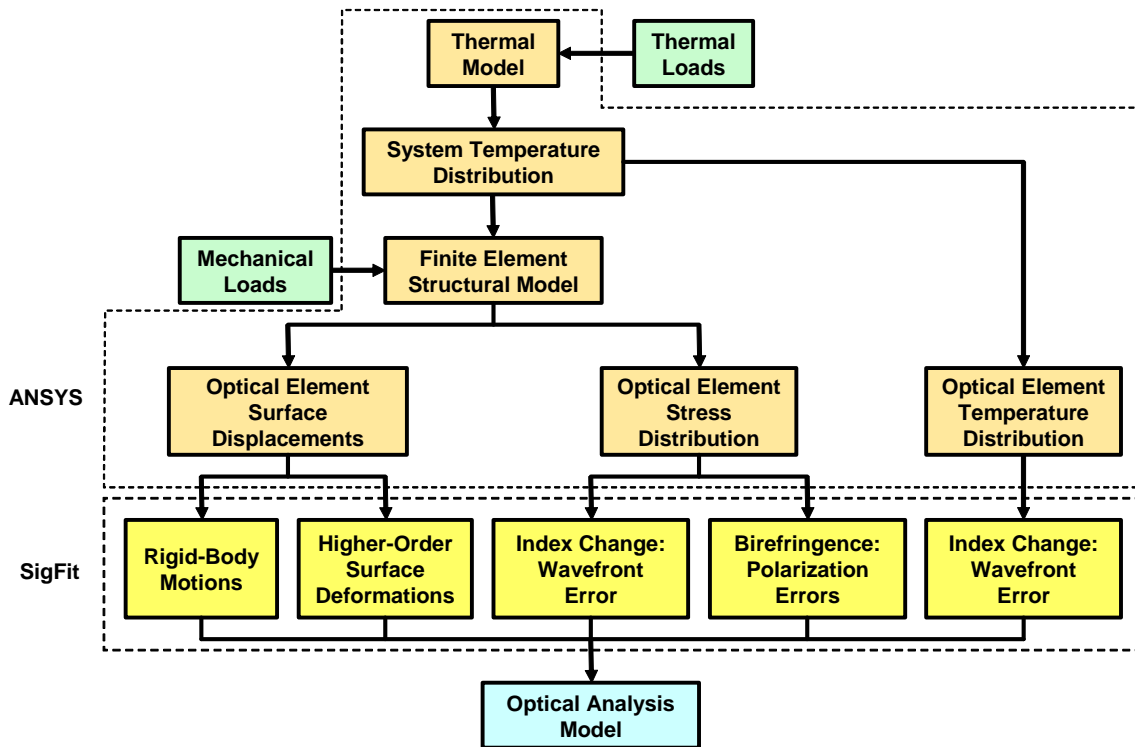

Figure 1.1: Flow chart of the process of optomechanical analysis of an optical system using ANSYS and SigFit.

2. Generation of Optical Thermal Loads

2.1 Irradience Predictions

Optical throughput analyses may be conducted in optical analysis software to predict the irradiences at any point in an optical system. These analyses may be performed with the surface and volumetric absorption within optical elements included so that the irradience predictions include the drop in irradiences through the optical system. Typically the irradience predictions are computed over the entrance and exit surfaces of each optical component and optionally at intermediate slice surfaces within transmissive optical components. The use of intermediate slice surfaces within a lens element is used to enhance the representation of the irradience pattern in the lens element beyond that represented by the irradience maps of the entrance and exit surfaces alone. These irradience predictions are formatted into arrays of data organized into rectangular grid arrays.

2.2 Calculation of Finite Element Heat Loads Due to Surface and Volumetric Absorption

Figure 2.2 shows the propagation of light through a medium labeled Region 1 into a medium labeled Region 2. A sample beam of incident power, P, of width a propagates through Region 1 and is incident on the interface between the two regions over an area c as shown. The sample beam has an angle of incidence, θ_{inc}, at the interface and a refracted angle, θ_{ref}, at a point on the interface whose normal

makes an angle, β, with the optical axis. The refracted beam leaves the interface with a width, b, and a power reduced by surface losses as given by the transmissibility of the interface surface, τ_s.
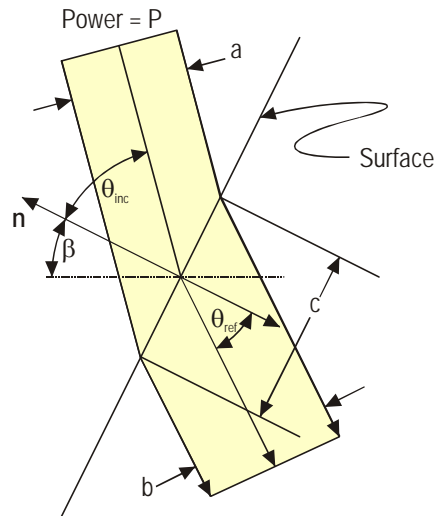

Figure 2.2: Propagation of light through the transition between two media.

Noting that $c = a/\cos(\theta_{inc}) = b/\cos(\theta_{ref})$ we may now write expressions for the surface flux, ϕ_s, and volumetric flux, ϕ_v, to be used in the calculation of surface and volumetric absorbed heat loads on the lens elements.

$$\phi_s = \Phi_{inc}\cos(\theta_{inc}) = \frac{P}{a}\cos(\theta_{inc}) = \frac{P}{c} \tag{2.1}$$

$$\phi_V = \Phi_{inc} = \frac{P}{a} = \frac{P}{c}\frac{1}{\cos(\theta_{inc})} \quad \text{Region 1} \tag{2.2a}$$

$$\phi_V = \Phi_{ref} = \frac{P\tau_s}{b} = \frac{P\tau_s}{c}\frac{1}{\cos(\theta_{ref})} \quad \text{Region 2} \tag{2.2b}$$

Note that the calculation of volumetric flux is different for each region due to the reduction in power and the change in beam size from a to b.

The situation illustrated in Figure 2.2 and the associated relationships in Eqns. 2.1 and 2.2 when applied to a real optical system only capture the behavior associated with illumination from a single field point. In reality illumination of the location shown in Figure 2.2 is composed of illumination from all field points. This results in an infinite sum of rays at unique powers, unique incidence angles, and unique infinitesimal width. In the limit as the width of all sample beams approach zero the full illumination is realized. In practice, however, field points of finite size are used and so the calculation of the fluxes becomes a finite sum of rays at unique powers, unique incidence angles, and unique finite widths. Therefore, we may write such sums for the calculation of the surface fluxes and volumetric fluxes over a finite domain on entrance surfaces, intermediate surfaces, and exit surfaces.

$$\phi_S = \frac{1}{c}\sum_{i=1}^{N} P_i \quad \text{Entrance and Exit Surfaces} \tag{2.3}$$

$$\phi_V = \frac{1}{c}\sum_{i=1}^{N} \frac{P_i}{\cos(\theta_{ref\,i})} \quad \text{Entrance Surfaces Only} \tag{2.4a}$$

$$\phi_V = \frac{1}{c}\sum_{i=1}^{N}\frac{P_i}{\cos\left(\theta_{ref\,i}\right)} = \frac{1}{c}\sum_{i=1}^{N}\frac{P_i}{\cos\left(\theta_{inc\,i}\right)} \quad \text{Intermediate Surfaces (No change in index)} \qquad (2.4b)$$

$$\phi_V = \frac{1}{c}\sum_{i=1}^{N}\frac{P_i}{\cos\left(\theta_{inc\,i}\right)} \quad \text{Exit Surfaces Only} \qquad (2.4c)$$

where, c is the surface area of the finite domain of the entrance surface, intermediate surface, or exit surface, N is the number of rays passing through the finite domain, P_i is the power of the ray from the ith ray after all prior losses (surface and volumetric) have been subtracted, $\theta_{ref\,i}$ is the angle of refraction from the surface normal of the ith ray, $\theta_{inc\,i}$ is the angle of incidence from the surface normal of the ith ray. Notice that in the calculation of the volumetric flux the angle of refraction is used for entrance surfaces while the angle of incidence is used for exit surfaces. For intermediate surfaces the angle of incidence is equal to the angle of refraction.

Once the surface and volumetric fluxes have been computed for all irradience maps, then the data may be used to compute the absorbed thermal loads to be applied to the finite element model. Figure 2.3 illsutrates this load generation process for surface absorption loads. The left-hand side of Figure 2.3 shows a rectangular array of incident fluxes computed using Eqn. 2.3 superimposed on a polar finite element mesh. Surface loads are computed for absorbing surfaces by multiplying the incident surface flux at each array point by its effective area and the surface absorption factor. This results in an absorbed power which is distributed to the nodes associated with the element face in which the array point lies. This load distribution is performed using the shape functions of the element face so that the correct distribution is reflected. Volumetric absorbed loads are computed in a fashion similar to that of surface absorbed loads.
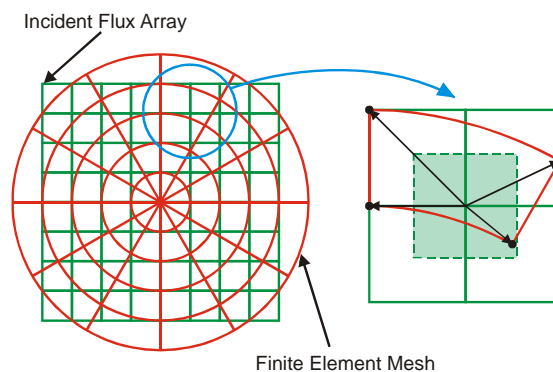

Figure 2.3: Illustration of distributing absorbed surface loads to a finite element mesh using shape function distribution.

Note that it is very important that the array of incident flux data be significantly finer in mesh size than the finite element model. If a coarse array of incident flux data is used then not all nodes in the finite element model will have thermal loads distributed to them. If a coarse array of incident flux data is to be used then standard finite element shape function interpolation methods may be employed rather than the finite element shape function distribution method shown in Figure 2.3.

3.   Thermo-optic Analysis Using ANSYS Generated Temperature Predictions

Changes in temperature of transmissive optics will change the index of refraction of the glass from which they are fabricated. These changes in refractive properties will alter how light travels through these optical components and will, therefore, affect optical performance. With thermal analyses performed in ANSYS we may conduct thermo-optic analyses to quantify the changes in optical performance due to these changes in temperature.

The temperature distributions computed in an ANSYS heat transfer analysis may be used as inputs to the thermo-optic analysis to determine an integrated optical path difference map for each lens

element. The integrated optical path difference map is computed by tracing integration paths through the finite element model of the lens and performing the OPD summation shown in Eqn. 3.1.

$$OPD = -\sum_{i=1}^{NINT} \Delta n_i \Delta L_i \tag{3.1a}$$

$$\Delta n_i = \int_{T_{ref}}^{T_i} \frac{dn(\tau)}{d\tau} d\tau \tag{3.1b}$$

where, *NINT* is the number of integration intervals along each path, $dn(\tau)/d\tau$ is the temperature dependent thermo-optic coefficient of the glass from which the lens is fabricated, T_i is the interpolated temperature at the ith integration point, T_{ref} is the reference temperature, and ΔL_i is the path length associated with the ith integration point.

The integration paths are formed by tracing paths from each node of the first surface of the lens element along a path defined by the apertures, A_{in} and A_{out}, of the two surfaces as shown in Figure 3.1. At each summation point along each path the temperature is determined by shape function interpolation from the finite element nodal temperatures predicted by ANSYS.
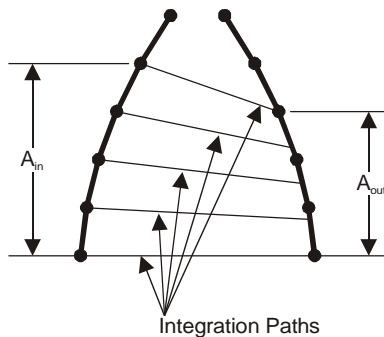

Figure 3.1: Illustration of how integration paths are defined for a lens element.

While these integration paths are approximations to the paths that real rays trace through the optical system, test cases have shown that for many systems this is a good approximation. Current work is focusing on providing a description of the three-dimensional nonuniform refractive index map directly to the optical analysis tools so that real rays may be traced to the full refractive index profile.

4. Surface Deformation Analysis Using ANSYS Generated Displacement Predictions

Deformation of optical components due to applied loads or changes in temperature will alter the shapes of their optical surfaces. Changes in the shapes of these optical surfaces will impact optical performance. With displacement predictions from ANSYS we may conduct surface deformation analyses to evaluate the impact on optical performance.

4.1 Surface Deformation as Represented By Finite Element Displacements

Nodal displacements of nodes lying on the optical surfaces in the finite element model consist of six vector components. A calculation for each node must be made to compute a surface deformation which represents the deformation of the surface experienced by the light incident on the surface. A normal surface deformation or a sag surface deformation may be computed depending on how the deformations are to be imported into an optical analysis tool. Illustration of the scalar sag surface deformation computed from the full nodal displacement vectors is shown in Figure 4.1.

The original node position, P, on the undeformed surface moves to the displaced node position, P'. However, a ray of light traveling along the axial direction which would hit the undeformed surface at point P hits the deformed surface at point A instead. The sag deformation at the undeformed location represented by the line segment PA cannot be exactly recovered but may be approximated by a result labeled ΔSag_{LIN}. An approximation of PA using a first-order Taylor series in the radial coordinate is

called the *linear corrected sag surface displacement* and is linearly related to the finite element displacement vector.
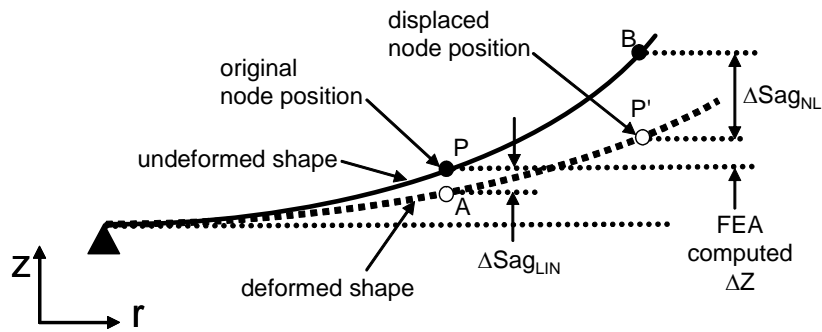

Figure 4.1: Illustration of sag deformations of a deformed optical surface.

Alternatively, the sag deformation BP′ labeled ΔSag_{NL} can be calculated exactly by subtracting the difference of the undeformed sags of points B and P from the axial displacement computed by the finite element analysis. However, this deformation is not linearly related to the finite element displacements. Therefore, this measure of sag deformation is referred to as the *nonlinear corrected sag surface displacement.* Use of this deformation can cause erroneous results if used with deformation descriptions which may be scaled significantly such as dynamic mode shapes of a vibrating system or actuator influence functions of an adaptively controlled system. In such analyses the linear corrected sag surface displacement must be employed. The use of the nonlinear corrected sag surface displacement is required, however, for accurate predictions when dealing with large displacement problems.

As an alternative to sag deformation the use of normal surface deformation may be employed. As shown in Figure 4.2, a ray of light traveling along the direction normal to the surface at P which would hit the undeformed surface at point P hits the deformed surface at point C. Like PA, PC must be approximated by a Taylor series.
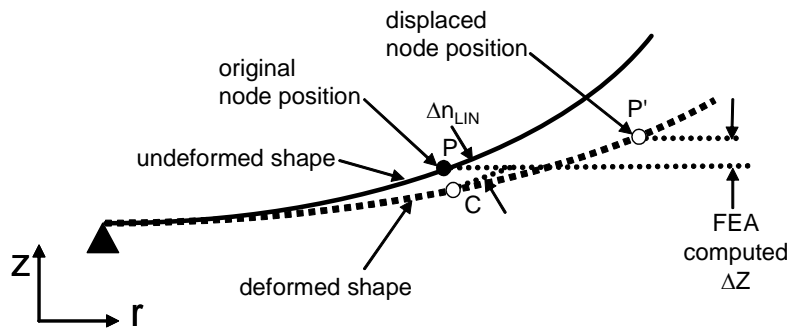

Figure 4.2: Illustration of sag deformations of a deformed optical surface.

Best fit rigid body motions may be computed from the surface deformation with the residual deformation described by two dimensional polynomial fits. Polynomials forms such as Zernike, XY, or asphere can be formatted into files readable by many commercially available optical analysis tools.

4.2   Calculation of Best Fit Rigid Body Motions of Surface Deformations

The best-fit rigid-body motions of an optical surface represented by a finite element mesh can be computed by assembling and solving a linear set of equations. An error metric, *E*, may be defined as the sum of the weighted squares of the differences between the actual nodal displacements, dx_i, dy_i, dz_i, and the nodal displacements associated with best-fit rigid-body motion, $d\tilde{x}_i, d\tilde{y}_i$, and $d\tilde{z}_i$.

$$E = \sum_i w_i (dx_i - d\tilde{x}_i)^2 + w_i (dy_i - d\tilde{y}_i)^2 + w_i (dz'_i - d\tilde{z}_i)^2 \qquad (4.1)$$

To find the best-fit motions ($T_x, T_y, T_z, R_x, R_y, R_z$), we minimize E, by taking partial derivatives with respect to each rigid body term and set each of the six result equations equal to zero. After setting all six derivatives to zero, there are six simultaneous equations to solve resulting in a solution to the best-fit rigid-body-motions.

4.3 Calculations of Polynomial Fits of Surface Deformations

The method of fitting surface polynomial terms to finite element data is a least squares fit to find the polynomial coefficients which minimize the error defined as,

$$E = \sum_{i=1}^{N} w_i \left(ds'_i - \sum_{j=1}^{M} C_j p_{ji} \right)^2 , \qquad (4.2)$$

where, N is the number of nodes, M is the number of polynomial terms, ds'_i is the surface deformation at node i, C_j is the polynomial coefficient for polynomial term j, p_{ji} is the value of normalized polynomial function for term j at node i. [3] Taking partial derivatives of E with respect to each polynomial coefficient and setting each equal to zero leads to a linear system of M equations for M unknowns,

$$[H]\{C\} = \{F\} \qquad H_{jk} = \sum_i w_i p_{ji} p_{ki} \qquad F_k = \sum_i w_i ds'_i p_{ki} \qquad (4.3)$$

which allows for computation of the coefficients which minimize the error E.

5. Stress Induced Birefringence Analysis Using ANSYS Generated Stress Predictions

States of stress within transmissive optical components will alter the their refractive performance. With stress predictions from ANSYS we may conduct stress-optic and birefringence analyses to evaluate the impact on optical performance.

The stress-optic properties are coefficients which relate the stress tensor to the change in impermeability as, [4]

$$\begin{Bmatrix} \Delta B_{11} \\ \Delta B_{22} \\ \Delta B_{33} \\ \Delta B_{12} \\ \Delta B_{23} \\ \Delta B_{31} \end{Bmatrix} = \begin{bmatrix} q_{11} & q_{12} & q_{13} & q_{14} & q_{15} & q_{16} \\ q_{21} & q_{22} & q_{23} & q_{24} & q_{25} & q_{26} \\ q_{31} & q_{32} & q_{33} & q_{34} & q_{35} & q_{36} \\ q_{41} & q_{42} & q_{43} & q_{44} & q_{45} & q_{46} \\ q_{51} & q_{52} & q_{53} & q_{54} & q_{55} & q_{56} \\ q_{61} & q_{62} & q_{63} & q_{64} & q_{65} & q_{66} \end{bmatrix} \begin{Bmatrix} \sigma_{11} \\ \sigma_{22} \\ \sigma_{33} \\ \sigma_{12} \\ \sigma_{23} \\ \sigma_{31} \end{Bmatrix} . \qquad (5.1)$$

Integration paths from the entrance surface to the exit surface are constructed as described above in Section 3. Along each path the principal changes in refractive index are found at each integration point along the path. These calculations are made using stresses interpolated from ANSYS nodal stress predictions to each integration point. The stress state at a single integration point is shown by an infintessimally small stress cube in Figure 5.1. The red ray indicates the path of the light ray passing through the lens.
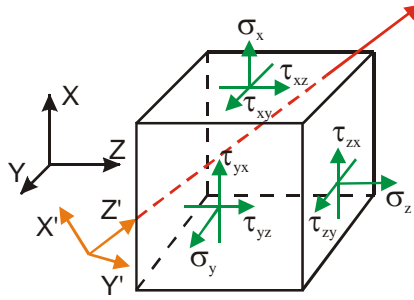
Figure 5.1: Light ray passing through an infintessimally small cube of stressed material.

The three-dimensional stress tensor predicted by ANSYS, σ, is first transformed to the ray coordinate system, X′,Y′,Z′, shown in orange in Figure 5.1. This results in the stress tensor σ'. The stress optic coefficient matrix, q, is then also transformed to this ray coordinate system resulting in q' using the transformation law of a fourth-order tensor. [5] The change in dielectric impermeability expressed in the ray coordinate system is then computed as,

$$
\begin{Bmatrix} \Delta B'_{11} \\ \Delta B'_{22} \\ \Delta B'_{33} \\ \Delta B'_{12} \\ \Delta B'_{23} \\ \Delta B'_{31} \end{Bmatrix} = \begin{bmatrix} q'_{11} & q'_{12} & q'_{13} & q'_{14} & q'_{15} & q'_{16} \\ q'_{21} & q'_{22} & q'_{23} & q'_{24} & q'_{25} & q'_{26} \\ q'_{31} & q'_{32} & q'_{33} & q'_{34} & q'_{35} & q'_{36} \\ q'_{41} & q'_{42} & q'_{43} & q'_{44} & q'_{45} & q'_{46} \\ q'_{51} & q'_{52} & q'_{53} & q'_{54} & q'_{55} & q'_{56} \\ q'_{61} & q'_{62} & q'_{63} & q'_{64} & q'_{65} & q'_{66} \end{bmatrix} \begin{Bmatrix} \sigma'_{11} \\ \sigma'_{22} \\ \sigma'_{33} \\ \sigma'_{12} \\ \sigma'_{23} \\ \sigma'_{31} \end{Bmatrix} .
\tag{5.2}
$$

The principal changes of index of refraction, $\Delta n''_1$ and $\Delta n''_2$, may be computed from the principal changes in impermeability. For a wavefront traversing a stress-induced birefringent medium, the changes in principal indices of refraction and their orientation vary along each integration path. An average optical path difference may be computed from these principal changes in refractive index. In addition, the integrated birefringent effects of this behavior may be computed using Jones calculus. [6] The magnitude and orientation of the effective birefringent properties of the stress field are derived from the system level Jones matrix assuming a linear retarder model. [7]

7.   Other Integrated Analysis Capabilities Using ANSYS and SigFit

Integration of the analysis capabilities of ANSYS with the analysis capabilities of optical analysis tools using SigFit extends into other analysis types as well as those discussed above. Equations for various optical performance metrics such as line-of-sight error can be written by SigFit into ANSYS constraint equations. Such equations can be used in design optimization analyses to allow constraints or optimization to be performed on optical performance metrics within the ANSYS environment. Natural frequency analysis results generated by ANSYS can be used within SigFit to predict optical performance due to random, harmonic, or transient loading. Predictions of the influence functions of actuators in an adaptively controlled system extracted from ANSYS analysis results using SigFit can be used in the simulation of the control of adaptive optics such as deformable mirrors and mirror arrays. [8, 9, 10]

6.   Example Analysis of a Lens System

A simple optical system was used to demonstrate the above analysis capabilities. The optical system, shown in Figure 6.1(a), is a double Gauss lens system. An optical model of the system was constructed in an optical analysis tool while a corresponding finite element model was constructed in ANSYS. The finite element model is shown in Figure 6.1(b).

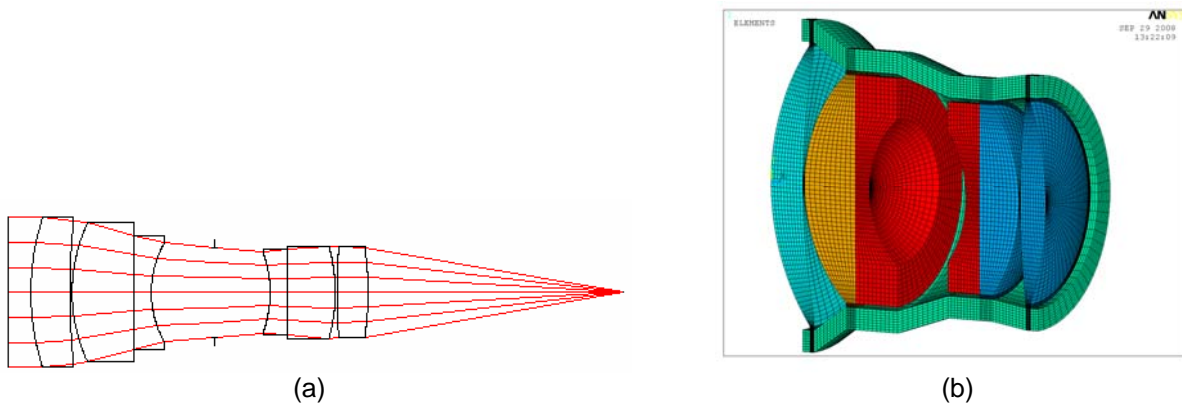<center>(a)   (b)</center>

Figure 6.1: Plot of (a) optical model of double gauss system with ray trace shown and (b) finite element model of double Gauss optical system constructed in ANSYS.

Irradiences were computed in the non-sequential raytrace capability of an optical analysis tool. Nodal thermal loads were computed using the method discussed in Section 2. These thermal loads were formatted into F,NODE,HEAT commands to be read into ANSYS. The thermal analysis was conducted to generate the temperature profile shown in Figure 6.2.
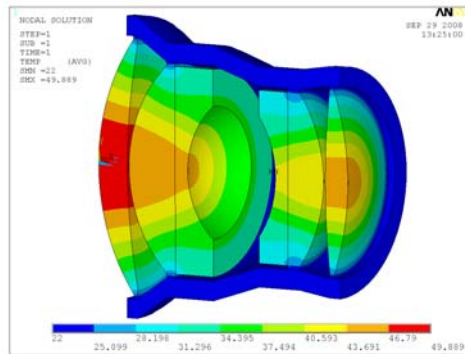

Figure 6.2: Plot of temperatures of double Gauss optical system expressed in degrees C.

The temperatures were used within SigFit to compute an OPD map associated with the thermo-optic effect for each lens element through the method discussed in section 3. These OPD maps were imported into a sequential raytrace model within an optical analysis tool in order to make the optical performance prediction of modulation transfer function shown in Figure 6.4(a). Modulation transfer function is a useful performance criterion in the design of an optical system that measures how well an imaging system is able to resolve the features of an object. The temperatures predicted by ANSYS were then used to perform a thermoelastic analysis to predict the displacements of the nodes on the optical surfaces of the lens elements. These displacement predictions were used within SigFit to develop optical surface deformation profiles using Zernike polynomials. These surface deformations were used within the optical analysis tool to generate the modulation transfer function shown in Figure 6.4(b).
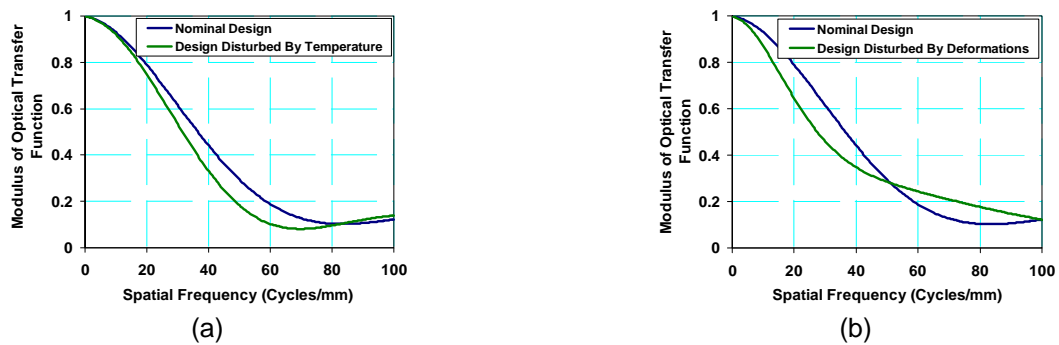
Figure: 6.4: Predictions of modulation transfer function of the nominal design compared to those due to (a) temperature changes and (b) thermoelastic surface deformations.

With stress predictions from the thermoelastic analysis birefringence was computed in SigFit and is plotted for the first lens element in Figure 6.5.
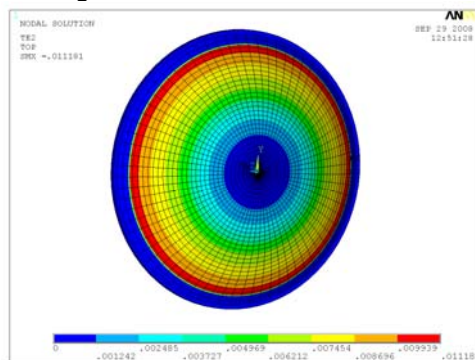

Figure 6.5: Prediction of birefringence generated in SigFit and plotted in ANSYS for lens element 1 due to thermoelastic stresses caused by light absorption. Units are in He-Ne waves/mm.

8.   Conclusion

The performance of an optical system is affected by mechanical disturbances in several different ways. Temperature changes of and induced stresses within transmissive optics and deformations of the optical surfaces of both refractive and reflective optical components affects optical performance. Prediction of the change in optical performance due to the expected mechanical disturbances simulated by ANSYS is extremely useful in the design development process.

9.   References

[1]   ANSYS is commercially available software from and a registered trademark of ANSYS, Inc.
[2]   SigFit is commercially available software from Sigmadyne, Inc.
[3]   V. Genberg, "Optical Surface Evaluation", SPIE Proc. Vol. 450, Conference on Structural Mechanics in Optical Systems, Nov 1983.
[4]   Nye, J. F., Physical Properties of Crystals: Their Representation by Tensors and Matrices, Oxford University Press, New York, 1985.
[5]   Shames, Irving H. and Francis A. Cozzarelli, Elastic and Inelastic Stress Analysis, Prentice Hall, Englewood Cliffs, NJ, 1992.
[6]   Jones, R. C., "A New Calculus for the Treatment of Optical Systems" J. Opt. Soc. Am., 31, 488-503, July, 1941.
[7]   Lu, Shih-Yau and Russel A. Chipman, "Homogeneous and inhomogeneous Jones matrices", J. Opt. Soc. Am. A/Vol. 11, No. 2/February 1994.
[8]   V. Genberg, K. Doyle, G. Michels, "Opto-Mechanical I/F for ANSYS", ANSYS, Canonsburg, PA, May, 2004.
[9]   G. Michels, V. Genberg, K. Doyle, G. Bisson, "Design optimization of actuator layouts of adaptive optics using a genetic algorithm", SPIE Vol. 5877 (22), San Diego, CA, August, 2005.
[10]   Doyle, Keith B., Victor L. Genberg , Gregory J. Michels, Integrated Optomechanical Analysis, SPIE Press, Bellingham, WA (2002).